# Boreal Forest Surface Parameterization in the ECMWF Model—1D Test with NOPEX Long-Term Data

D. GUSTAFSSON,* E. LEWAN,+ B. J. J. M. VAN DEN HURK,# P. VITERBO,@ A. GRELLE,& A. LINDROTH,**
E. CIENCIALA,++ M. MÖLDER,** S. HALLDIN,## AND L.-C. LUNDIN##

*Department of Land and Water Resources Engineering, Royal Institute of Technology, Stockholm, Sweden
+Division of Environmental Physics, Department of Soil Sciences, SLU, Uppsala, Sweden
#KNMI, De Bilt, Netherlands
@European Centre for Medium-Range Weather Forecasts, Shinfield Park, Reading, Berkshire, United Kingdom
&Department for Production Ecology, SLU, Uppsala, Sweden
**Department of Physical Geography, Lund University, Lund, Sweden
++Institute of Forest Ecosystem Research, Jilove u Prahy, Czech Republic
##Department of Hydrology, Uppsala University, Uppsala, Sweden

(Manuscript received 24 January 2002, in final form 26 June 2002)

ABSTRACT

The objective of the present study was to assess the performance and recent improvements of the land surface scheme used operationally in the European Centre for Medium-Range Weather Forecasts (ECMWF) in a Scandinavian boreal forest climate/ecosystem. The previous (the 1999 scheme of P. Viterbo and A. K. Betts) and the new (Tiled ECMWF Surface Scheme for Exchange Processes over Land, TESSEL) surface schemes were validated by single-column runs against data from NOPEX (Northern Hemisphere Climate-Processes Land-Surface Experiment). Driving and validation datasets were prepared for a 3-yr period (1994–96). The new surface scheme, with separate surface energy balances for subgrid fractions (tiling), improved predictions of seasonal as well as diurnal variation in surface energy fluxes in comparison with the old scheme. Simulated wintertime evaporation improved significantly as a consequence of the introduced additional aerodynamic resistance for evaporation from snow lying under high vegetation. Simulated springtime evaporation also improved because the limitation of transpiration in frozen soils was now accounted for. However, downward sensible heat flux was still underestimated during winter, especially at nighttime, whereas soil temperatures were underestimated in winter and overestimated in summer. The new scheme also underestimated evaporation during dry periods in summer, whereas soil moisture was overestimated. Sensitivity tests showed that further improvements of simulated surface heat fluxes and soil temperatures could be obtained by calibration of parameters governing the coupling between the surface and the atmosphere and the ground heat flux, and parameters governing the water uptake by the vegetation. Model performance also improved when the seasonal variation in vegetation properties was included.

## 1. Introduction

Land surface energy fluxes constitute the lower boundary for the physical processes in the atmosphere. Adequate formulations and parameterization of land surface processes are thus essential for significant improvements of operational models for climate and weather predictions. Thorough testing of the surface schemes in offline mode (i.e., decoupled from the complex interactions in the full 3D model) has been stressed, as well as the need for tests with respect to seasonal timescales (Viterbo and Beljaars 1995; Henderson-Sellers 1996; Chen et al. 1997; Verseghy 2000). Verseghy (2000) also emphasized the importance of addressing the ability to reproduce fluxes from homogeneous surfaces prior to tests for heterogeneous surfaces at regional and global scales. The evaluation of land surface schemes for different ecosystems has still been rather limited, because of the lack of suitable datasets.

The boreal forests at high latitudes have a great influence on the annual and seasonal climatology of the Northern Hemisphere by reducing the otherwise high albedo of snow-covered areas during winter and by affecting the partitioning of net radiation between sensible and latent heat fluxes at all times of the year. Several experiments with global circulation models (e.g., Bonan et al. 1992; Thomas and Rowntree 1992; Douville and Royer 1997; Viterbo and Betts 1999) have shown that the boreal forests increase surface air temperature, latent heat flux, and atmospheric moisture over the whole Northern Hemisphere when compared with a deforested surface. The impact of these effects is largest in spring

*Corresponding author address:* Elisabet Lewan, Department of Soil Sciences, Swedish University of Agricultural Sciences, Ulls väg 17, Ultuna, Box 7014, S–750 07 Uppsala, Sweden.
E-mail: lisbet.lewan@mv.slu.se

in the Arctic and subarctic regions, but extends in time throughout the year and spatially toward the Tropics. The boreal forests also have an important influence on the long-term budgets of atmospheric carbon dioxide and methane. Bonan et al. (1995) showed that these biochemical interactions are more important for the climate at long timescales, when redistribution of vegetation due to climate change is taken into account.

The surface scheme introduced operationally in August 1993 at the European Centre for Medium-Range Weather Forecasts (ECMWF) was presented by Viterbo and Beljaars (1995). This scheme was subsequently modified in September 1996 to account for soil freezing (Viterbo et al. 1999) and in December 1999 to account for the albedo of boreal forest (Viterbo and Betts 1999)—and is hereinafter referred to as VB95. It is based on the heat and water budgets for four active soil layers plus an additional surface layer with four subgrid surface fractions: bare soil, vegetation, snow, and interception layer, with one surface temperature in common. The scheme was evaluated within the Project for Intercomparison of Land-Surface Parameterization Schemes (Henderson-Sellers et al. 1993), and was tested with data from the First ISLSCP (International Land Surface Satellite Climatology Project) Field Experiment, tall grass prairie, United States (Betts et al. 1998a), Cabauw (grassland, Netherlands) (Bosveld et al. 1999), Amazonial Regional Meteorological Experiment, rainforest, Brazil (Viterbo and Beljaars 1995), and recently also the BOREAS (Boreal Ecosystem–Atmosphere Study, Canada) experiments (Betts et al. 1998a). These studies revealed a number of shortcomings in the scheme and emphasized the need for more realistic descriptions of different vegetation types (Douville et al. 1998; van den Hurk et al. 2000).

Consequently the land surface parameterization scheme was redesigned and a new scheme was put into operation in June 2000, hereinafter referred to as the Tiled ECMWF Surface Scheme for Exchange Processes over Land (TESSEL). A description of the scheme and the most important changes can be found in van den Hurk et al. (2000). The new scheme includes six land tiles: bare soil, high vegetation, low vegetation, high vegetation with snow beneath, snow on low vegetation, and an interception layer. The energy balance is solved separately for each tile, giving individual surface temperatures for different surface fractions. The VB95 and the TESSEL schemes were evaluated in offline mode against data from seven land surface experiments representing different climate regions and vegetation types, including a long-term dataset from the BOREAS experiment (van den Hurk et al. 2000).

Betts et al. (1998b) and van den Hurk et al. (2000) concluded that evaporation rates over boreal forests were overestimated by the VB95 scheme in winter, spring, and summer in comparison with data from BOREAS. The discrepancies were mainly attributed to an overestimation of evaporation from snow and the neglect of the influence of frozen soil and vapor pressure deficit on transpiration (Betts et al. 1999).

Comparison of the VB95 and TESSEL schemes with long-term flux data from the BOREAS Northern Study Area (BOREAS NSA) showed significant improvements of simulated heat fluxes (van den Hurk et al. 2000). These improvements were ascribed to the introduction of a separate energy budget for the snow layer, an additional aerodynamic resistance within the canopy above the snow layer, the limitation of water extraction in frozen soil, and the inclusion of a vapor pressure deficit response function for transpiration.

The objective of the present study is to make an independent assessment of the performance and recent improvements of the ECMWF land surface scheme with respect to boreal forest using long-term flux data from the NOPEX (Northern Hemisphere Climate-Processes Land-Surface Experiment; Halldin et al. 1998, 1999). The climate of the NOPEX study area is warmer when compared with the more continental climate of the BOREAS area referred to above. The annual mean air temperature is 5.5°C (Uppsala, 1961–90; Lundin et al. 1999) as compared with −3.4°C in BOREAS NSA (Thompson, Manitoba, Canada, 1968–89; Lafleur et al. 1997). The largest difference in air temperature occurs during winter: the mean daily air temperatures in January are −3.6° and −25°C for NOPEX and BOREAS, respectively. However, the mean annual precipitation is rather similar for the two areas (527 mm in Uppsala and 536 mm in Thompson), of which the largest proportion occurs in summer and autumn. On average, summers are somewhat drier in the NOPEX area, where 59% of the annual precipitation occurs in May–October as compared with 73% for BOREAS.

The VB95 and the TESSEL surface schemes were evaluated based on single-column runs with data from the NOPEX Central Tower site. The models were parameterized based on the standard parameter values generally used within the operational 3D versions of the models. Forcing and validation datasets were prepared for a 3-yr period (1994–96) and the models were run for the whole period with a 30-min time step. We focused on comparisons with measured latent and sensible heat fluxes that represent aggregated areal fluxes (Grelle 1997). However, comparisons with the observed temporal variation in more local-scale data (soil water content, soil temperature, ground heat flux, and stand transpiration) are also presented, since these contribute to an understanding of improvements and limitations in the present land surface scheme. In order to identify periods during which the dynamic representation of the surface was of major importance for model performance, the seasonal variation in evapotranspiration of the new and the old scheme was compared with that obtained with a simple Penman–Monteith formulation.

## 2. Material and methods

### *a. Model description*

A brief description of the present (TESSEL) and previous versions (VB95) of the land-surface scheme op-

TABLE 1. Major differences between VB95 and the TESSEL surface schemes in the ECMWF model.

| Concept | VB95 | TESSEL |
|---|---|---|
| Subgrid fractions over land (tiles) | 4 (bare soil, vegetation, snow, intercepted water) | 6 (bare soil, low vegetation, high vegetation, snow on low vegetation, high vegetation with snow beneath, intercepted water) |
| Surface temperature | Common for all tiles | 1 for each tile |
| Vegetation characteristics | 1 global parameter set | Dependent on vegetation type |
| Transpiration, controlled by: | Total soil moisture and radiation | Unfrozen soil moisture, radiation and vapor pressure deficit |
| Vegetation albedo | Fixed | Seasonal course |
| Snow layer | Thermally mixed with the upper soil layer | Independent thermal content |
| Snow albedo | Fixed | Varies with snow age and tile |
| Bare soil evaporation | Relative humidity concept, $\alpha$ scheme* | Surface resistance concept, $\beta$ scheme* |

* See, for example, Mahfouf and Noilhan (1991).

erational in the ECMWF will be given here. Further details can be found in Viterbo and Beljaars (1995) and van den Hurk et al. (2000).

Both versions simulate the water and heat budgets for a vertical soil column discretized into four layers (7, 21, 72, and 189 cm in thickness), based on two coupled differential equations: the Richards equation and Fourier law of diffusion. In offline mode both schemes are forced by near-surface observed weather variables (wind speed, air temperature, air humidity, incoming shortwave and longwave radiation, and precipitation). A ''skin layer'' (on top of the soil column) with zero heat capacity is in instantaneous equilibrium with its forcing; that is, the skin temperature is calculated by solving the surface energy balance equation:

$$R_n = H + \mathrm{LE} + G, \tag{1}$$

where $R_n$ is the net radiation (W m$^{-2}$), $H$ and LE are the turbulent heat fluxes of sensible and latent heat (W m$^{-2}$), and $G$ is the ground heat flux (W m$^{-2}$). Here $R_n$ and $G$ are defined as positive downward and $H$ and LE as positive upward. The ground heat flux between the skin layer and the topsoil layer is governed by an empirical parameter, the skin layer heat conductivity, which has values corresponding to about 10%–20% of the soil thermal conductivity at field capacity. Bottom boundary conditions are zero heat flux and free drainage. The aerodynamic resistances for the turbulent exchange are based on an iterative transformation of Richardson's number into the Monin–Obukhov stability parameter ($z/L$) (Beljaars and Holtslag 1991). Total surface energy fluxes are the sum of fluxes from the different subgrid surface fractions (tiles), weighted by their areal fractions.

The major changes between the VB95 and the TESSEL scheme concern the treatment and concepts for different tiles—especially with respect to snow and vegetation. The most important differences are summarized in Table 1 and in Fig. 1 and are briefly commented upon below.

The VB95 scheme had four tiles (Table 1) for which a common skin layer temperature was calculated by solving the grid surface energy balance [Eq. (1)] (Viterbo and Beljaars 1995). In TESSEL the water and heat fluxes are calculated separately for each tile, giving individual surface temperatures for each subgrid fraction. The tiles for vegetation and snow have been differentiated into four new tiles (Table 1). The skin layer conductivity is now tile dependent (Fig. 1), and the aerodynamic resistance and the vapor pressure at the surface are based on the skin temperature for each tile. Evaporation from high vegetation with snow beneath is calculated from both the canopy and the snow component, where evaporation from the snowpack is based on an additional aerodynamic resistance (Fig. 1). Bare soil evaporation has been changed from a relative humidity concept to a surface resistance approach.

In TESSEL, the snowpack (previously merged into the top soil layer) is treated as an additional layer on top of the soil column, with a specific snow temperature. The heat flux from the snow to the topsoil layer is calculated with a resistance approach. The snow albedo (which is fixed in VB95) varies with snow age (0.85–0.50), except for tiles with high vegetation with snow beneath for which it is fixed to 0.20. The snow-free albedo in VB95 is time-invariant, while in TESSEL it follows a prescribed climatological cycle. In VB95 all radiation is absorbed in the skin layer, whereas in TESSEL 3%–5% of the net shortwave radiation is transmitted through the canopy (high or low) to the topsoil or the snow layer. In addition, the energy absorbed/released by melting/freezing of soil water has been included in the soil thermal budget.

The VB95 scheme had only one set of vegetation parameters, thus representing a single type of vegetation. TESSEL has a coverage map of 15 different vegetation types (e.g., short grass, tall grass, annual crop, deciduous broad leaf trees, evergreen shrubs, evergreen needle-leaf trees). Vegetation specific values are chosen for leaf area index (LAI), fractional vegetation coverage, minimum canopy resistance, sensitivity coefficient for vapor pressure deficit, and root distribution. In contrast to the previous version, transpiration is also governed

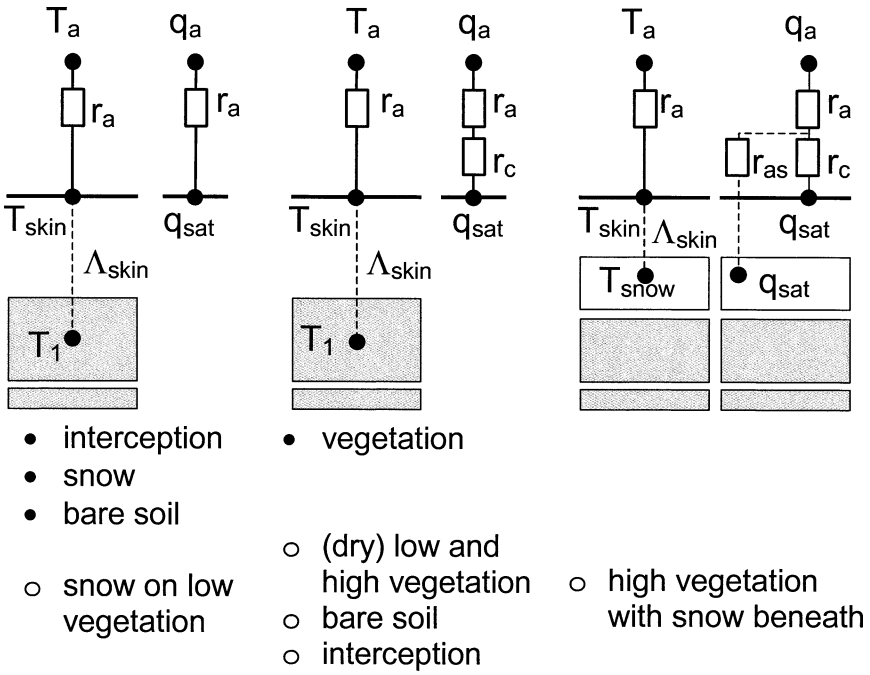


FIG. 1. Resistance scheme for three types of coupling between the surface and the atmosphere (from van den Hurk et al. 2000). The list below each scheme refers to the subgrid fraction types (tiles) in the VB95 (black dots) and the TESSEL (circles) models.

by vapor pressure deficit and is limited in frozen soil (Table 1).

### *b. Field site*

The central NOPEX experimental site (60.5°N, 17.29°E, altitude 45 m) on Norunda Common, about 30 km north of Uppsala, Sweden, is located in the southern part of the boreal forest zone (Halldin et al. 1998, 1999). The surrounding area consists of 70–100-year-old forest dominated by Norway spruce (*Picea abies*) and Scots pine (*Pinus sylvestris*) of rather uniform height (25–30 m). The canopy has a leaf area index between 3 and 5. The soil is a deep boulder-rich sandy till of glacial origin. The region is flat and homogeneous with a maximum fetch of 6 km extending to the southwest and a minimum fetch determined by a clearing and a small lake at 1 km distance from the central mast toward the north–northwest. The mean air temperature is 5.5°C (Uppsala, 1961–90), the mean annual precipitation is 527 mm, and the mean Penman open-water evaporation is 454 mm (Lundin et al. 1999).

### *c. Forcing data*

The continuous climate-monitoring program at this site has been running since the beginning of June 1994. Atmospheric fluxes of heat and moisture, shortwave and longwave radiation, and meteorological variables were measured in the 102-m mast, at the center of the site. Soil moisture and temperature, soil heat flux, and stem sap flow were measured in the 70- and 100-year-old forest stands as described by Lundin et al. (1999).

Air temperature, wind speed, and air humidity were obtained at 35-m height. Missing data were replaced with observations from Uppsala Airport, about 30 km south of Norunda, after corrections based on linear regression between the stations. Downward shortwave radiation was measured at 102-m height and longwave radiation at 68-m height (Mölder et al. 1999b). For periods of missing data, longwave radiation was estimated as a function of air temperature, vapor pressure, and cloudiness (Konzelmann et al. 1994). Missing shortwave radiation was estimated with Ångström's formula (Ångström 1924), using cloudiness from Uppsala Airport as input. Precipitation was measured at Norunda in a small clearing with a specially designed rain gauge that minimizes the systematic errors due to wind and wetting losses (Seibert and Morén 1999). However, precipitation was only measured during summer. Winter precipitation was therefore estimated from observations at Uppsala Airport made with conventional rain gauges. The precipitation was assumed to consist of snow at air temperatures below −2°C, as rain above 2°C, and as a mixture (linear proportions) of rain and snow at air temperatures between −2° and 2°C. Winter precipitation was systematically corrected by +15% for snowfall and +7% for rainfall (Eriksson 1983). In general, the meteorological forcing data are of high quality, especially during summer periods (May–October). During winter, measured air humidity was occasionally higher than

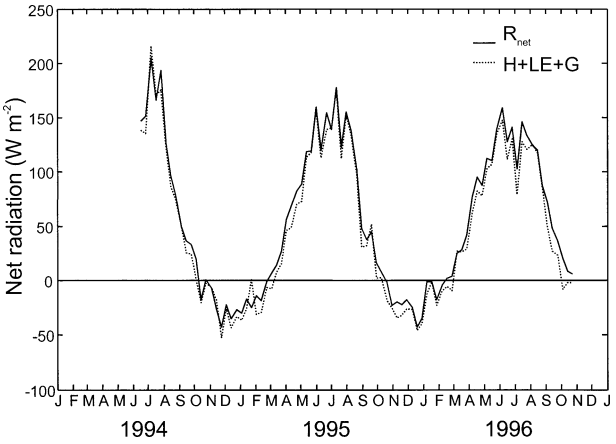


FIG. 2. Measured net radiation and sum of measured sensible, latent, and ground heat flux (10-day averages).

could be expected from the corresponding saturated vapor pressure. For such cases, the saturated humidity value was used instead. The data, functions, and instruments used for the meteorological forcing are summarized in the appendix.

### *d. Validation data*

Sensible and latent heat fluxes were obtained from eddy-correlation measurements at 35-m height (Grelle and Lindroth 1996; Grelle 1997) using a sonic anemometer, a fast-response platinum thermometer, and a closed-path gas analyzer. The sonic anemometer was calibrated to correct for flow distortion and the turbulent fluxes were corrected for sensor inclination, signal time lag caused by the length of the sampling tube, frequency loss caused by both tube attenuation and sensor-response time, and air-density fluctuations because of sensible heat fluxes (Grelle and Lindroth 1996). Net radiation was obtained from net radiometers at 68- (96%) and 98- (4%) m height (Mölder et al. 1999b) and soil heat flux from measurements with heat flux plates at 6-cm depth at two locations (Kellner et al. 1999). The sum of turbulent heat fluxes and the soil heat flux constituted 86% of the observed net radiation, when averaged over the total available dataset (Fig. 2). During summer periods the accumulated energy balance closure was 96% (Grelle and Lindroth 1996). It should be emphasized that a full closure of the energy balance could not be expected since the observed components represent different footprint areas. The measured net radiation represents a rather limited area around the mast, whereas the eddy-correlation fluxes represent a larger footprint from different areas depending on wind direction and atmospheric stability, especially during winter (Grelle 1997). A source area analysis following Schmid (1994) indicates that the daytime fluxes originate from an area between 50 m and 1 km from the mast, whereas the source area of the nighttime fluxes is spread up to tens of kilometers from the mast (Grelle 1997).

Liquid soil water content and soil temperature were measured with time-domain reflectometry and thermocouples in 14 profiles at 5–6 depths down to 100 cm (Kellner et al. 1999). The profile measurements were averaged and integrated over the depths of the model layers to generate comparable variables. The variation between soil profiles was high, especially for the soil water content.

Transpiration data were obtained from sap flow measurements on individual trees scaled to represent the average stand transpiration (Cienciala et al. 1999). Daily average values of sap flow measurements are a good estimate of daily transpiration. However, at shorter (diurnal) timescales, sap flow measurements show a significant time lag, due to the storage of water in the tree.

The validation data are summarized in Table 2 and the instruments are given in the appendix.

TABLE 2. Variables used for the evaluation of the ECMWF surface models. Periods are displayed in year (19XX), month, day format (yymmdd).

| Variable | Location | Period | Capture fraction* | Comment |
|---|---|---|---|---|
| Latent heat flux (W $m^{-2}$) | 35 m | 940611–961031 | 95% | |
| Sensible heat flux (W $m^{-2}$) | 35 m | 940611–961031 | 95% | |
| Net radiation (W $m^{-2}$) | 68 m (96%)<br>98 m (4%) | 940611–961031 | 95% | |
| Soil heat flux (W $m^{-2}$) | 6-cm depth | 940611–961031 | 95% | Average of four plates in two locations |
| Tree sap flow (mm $day^{-1}$) | Measurements on trees within 30 m from the central tower, scaled to represent stand transpiration | 950704–950831 | 100% | Within-day values |
| | | 940617–941031 | 85% | Daily averages |
| | | 950422–951028 | 100% | Daily averages |
| | | 960423–961024 | 83% | Daily averages |
| Soil temperature (°C) | 6 levels<br>0–100 cm | 940605–961231 | 96% | Average of 14 soil profiles, integrated over the model layer depths |
| Soil moisture ($m^3$ $m^{-3}$) | 6 levels<br>0–100 cm | 940610–961231 | 95% | Cf. soil temperature |

* Percentage of time coverage within the measuring period.

TABLE 3. Model parameter values for the old and the new version of the ECMWF surface scheme, used in the simulations for the NOPEX boreal forest. Figures in boldface represent values based on site-specific observations.

| Parameter | VB95 | TESSEL | |
|---|---|---|---|
| | | High vegetation | Low vegetation |
| Vegetation coverage | **0.90** | **0.90** × 0.986 | **0.90** × 0.014 |
| LAI | 4 | 5 | 3 |
| Minimum canopy resistance (s $m^{-1}$) | 60 | 100 | 60 |
| Sensitivity coef to VPD ($hPa^{-1}$) | — | 0.03 | 0 |
| Root distribution (four layers) (%) | 33, 33, 33, 0 | 26, 39, 29, 6 | 24, 41, 31, 4 |
| Skin conductivity (W $m^{-2}$ $K^{-1}$) | 15 | 20 (unstable)<br>9.5 (stable) | 10 |
| Skin conductivity—bare soil | 15 | 15 | |
| Skin conductivity—intercepted water | 15 | 10 | |
| Roughness (momentum) (m) | **1.75** | **1.75** | **1.75** |
| Roughness (heat) (m) | 0.175* | 0.175* | 0.175* |
| Albedo (vegetation) | **0.08** | **0.0815–0.0965** | |
| Albedo (snow) | 0.20 (vegetation)<br>0.70 (other) | 0.20 (high vegetation)<br>0.50–0.85 (other) | |
| Height ($z$) over displacement height (m) | **13.9** | **13.9** | |
| Interception capacity (m $LAI^{-1}$) | 0.0002 | 0.0002 | |
| Interception efficiency | 0.5 | 0.5 | |
| Soil porosity ($m^3$ $m^{-3}$) | 47.2 | 47.2 | |
| Water content at field capacity ($m^3$ $m^{-3}$) | 32.3 | 32.3 | |
| Water content at wilting point ($m^3$ $m^{-3}$) | 17.1 | 17.1 | |
| Matric potential at saturation (m) | −0.338 | −0.338 | |
| Hydraulic conductivity at saturation (m $s^{-1}$) | $4.57 \times 10^{-6}$ | $4.57 \times 10^{-6}$ | |

* ECMWF praxis.

### *e. Model parameterization*

Model parameters were set according to values generally used within the operational 3D version of the ECMWF model corresponding, in the case of geographically dependent parameters, to the value at the closest grid point. For the new scheme, the relative area of high and low vegetation was 0.986 and 0.014, respectively. The total fractional vegetation cover was set to 0.90 in both schemes. However, vegetation albedo, vegetation roughness length for momentum, and displacement height were based on measurements from the NOPEX area (Mölder and Lindroth 1999; Mölder et al. 1999a,b). The values chosen for each of the surface schemes are summarized in Table 3.

The surface schemes were run in offline mode for a 3-yr period (1 January 1994–19 December 1996), at a 30-min time step. Initial soil moisture and temperature profiles were obtained by running the model three times in sequence for the first year (1994). The first of these runs used uniform soil profiles as initial conditions (soil moisture content = 0.323 $m^3$ $m^{-3}$ and soil temperature = 5°C). The final values of the soil state variables obtained from these runs were used as initial conditions for the 1994–96 simulations presented in the following. No calibration was done.

### *f. Model evaluation*

Simulated fluxes were compared with observed surface energy balance components, net radiation, sensible heat flux, latent heat flux, and ground heat flux [Eq. (1)]. The comparisons focused on long-term seasonal variations. Discrepancies between simulated and measured fluxes were also examined with respect to temporal dynamics in soil temperature, soil water content, stand transpiration and the degree of atmospheric and/or surface control. The results are discussed in relation to the major recent changes of the ECMWF surface scheme and its parameterization.

The effect of a dynamic representation of the land surface is most significant when the surface control is large in comparison with the atmospheric forcing—for example, during droughts. Such periods were identified by comparing the observed and simulated evapotranspiration with that obtained from a simple Penman formulation (Penman 1953) as modified by Monteith (1965), with a constant surface resistance:

$$\mathrm{LE} = \frac{\Delta(R_n - G) + \rho c_p \dfrac{\delta e}{r_a}}{\Delta + \gamma^*}, \tag{2}$$

where $\delta e$ is the vapor pressure deficit (Pa) at the observation height, $\Delta$ is the slope of saturation pressure vs temperature (Pa $K^{-1}$), $\rho$ is the air density (kg $m^{-3}$), $c_p$ is the specific heat of air (J $kg^{-1}$ $K^{-1}$), and

$$\gamma^* = \frac{\gamma(r_a + r_s)}{r_a}, \tag{3}$$

where $\gamma$ is the psychrometric constant 66 (Pa $K^{-1}$), $r_a$ (s $m^{-1}$) is the aerodynamic resistance, and $r_s$ (s $m^{-1}$) is a surface resistance.

Latent heat flux was calculated at daily resolution

TABLE 4. Mean air temperature and precipitation during the simulation period.

| Year | Mean air temperature (°C) | Precipitation (mm) |
|---|---|---|
| 1994 | 5.9 | 537 |
| 1995 | 5.4 | 550 |
| 1996 | 4.8 | 528 |

using climate data from the Norunda site, a constant surface resistance, and assuming the ground heat flux to be negligible. The aerodynamic resistance was based on the same roughness values as used in the model runs, assuming neutral atmospheric stability. The surface resistance (195 s $m^{-1}$) was inferred from calibrating the model with the observed latent heat flux (1994–96), to represent the average surface control on evaporation. Periods during which the Penman–Monteith (P–M) evapotranspiration was significantly higher than that obtained from the simulations and measurements demonstrate when evapotranspiration was mainly controlled by soil moisture conditions.

An additional sensitivity test was performed with the TESSEL model in order to better understand the causes of the differences between the two models and the remaining discrepancies between the TESSEL simulations and the observations. Some key parameters were varied (skin layer conductivity, roughness length for heat, minimum canopy resistance, and leaf area index), based on the findings of the original simulations.

## 3. Results

### a. Climatic conditions

The period examined included both dry and wet summers as well as mild and cold winters. Annual precipitation (Table 4) was similar but the within-year distribution differed between years (Fig. 3). Summer 1994 was warm and dry; summer 1995 was initially warm and humid but changed to drier conditions at the end, whereas summer 1996 was rather wet. The 1994/95 winter was mild and humid, in contrast to the 1995/96 winter, which was cold and dry.

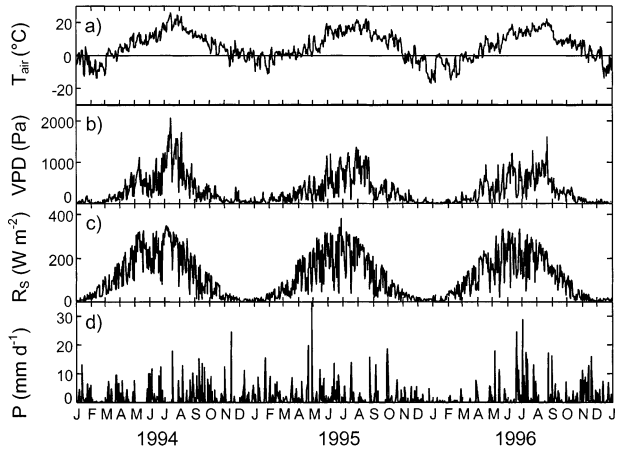


FIG. 3. Weather conditions during the 3 yr of simulation: (a) air temperature, (b) vapor pressure deficit, (c) global radiation, and (d) precipitation (daily average values).

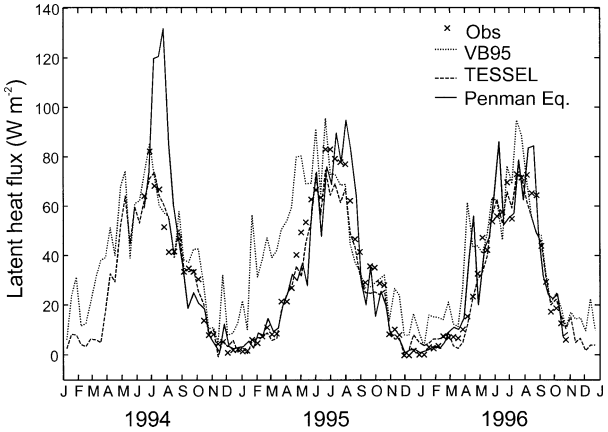


FIG. 4. Simulated and measured latent heat flux (10-day averages).

### b. Simulated and measured surface fluxes—A quick overview

Seasonal dynamics in surface energy fluxes compared significantly better to observed values when simulated with the new scheme (TESSEL) as opposed to the old one (VB95). Latent heat flux was systematically overestimated in winter, spring, and early summer by the old scheme (Fig. 4). The new scheme significantly improved the prediction of latent heat flux and, as a consequence, the seasonal variation in sensible heat flux was also improved (Fig. 5). However, the new scheme still revealed some systematic discrepancies. The sensible heat flux from the air to the surface was underestimated in winter. This discrepancy was linked to a compensating overestimation of the heat flux from the

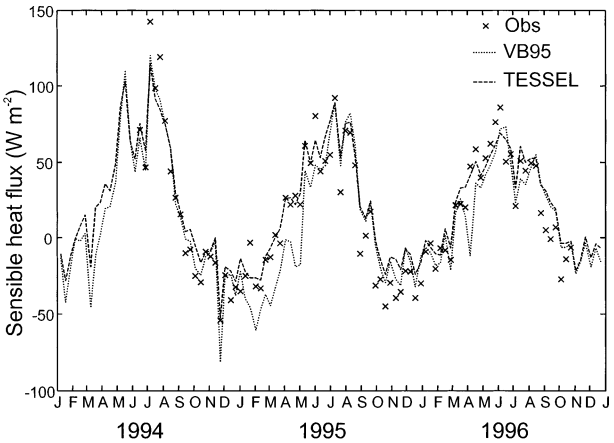


FIG. 5. Simulated and measured sensible heat flux (10-day averages).

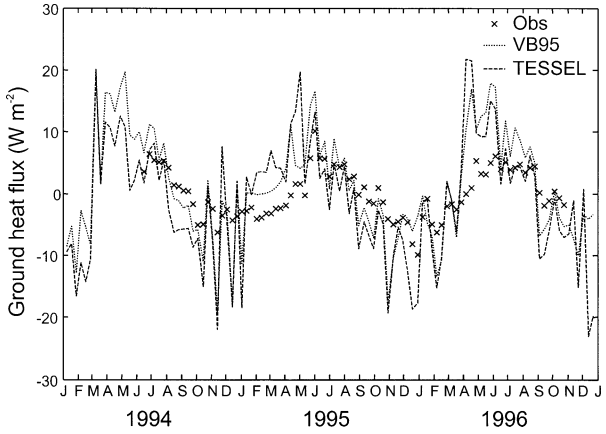


FIG. 6. Simulated and measured ground heat flux (10-day averages).

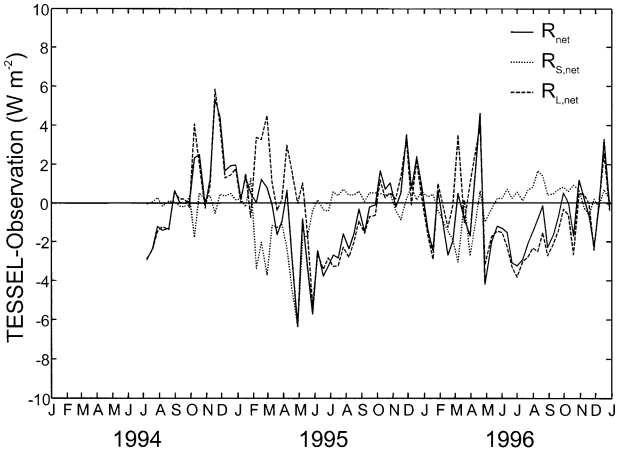


FIG. 7. Discrepancy between simulated (TESSEL) and measured net shortwave radiation, net longwave radiation, and net radiation (10-day averages).

ground to the surface during the same period (Fig. 6). Simulated and measured net radiation agreed well in general (Fig. 7). Discrepancies could be related to small overestimations of surface temperature in summer and albedo in winter.

The significance of different changes of the land surface scheme for predicted surface energy fluxes is discussed below.

### *c. Latent heat flux—The role of snow evaporation*

The VB95 scheme largely overestimated latent heat flux from the snow cover, which was the reason behind the general overestimation of latent heat flux in winter and early spring (Figs. 4 and 8). The overestimation was worse in 1994/95, probably because of warm and humid weather with a higher frequency of neutral conditions and thus generally higher values of the exchange coefficients in comparison with the colder and more stable conditions in 1995/96 (Figs. 8c,d). The introduction of a separate energy balance over snow-covered areas and an additional aerodynamic resistance for evaporation from snow under the tree canopy (TESSEL) significantly improved the predictions of latent heat flux during these periods (Fig. 4).

### *d. Sensible heat flux and ground heat flux*

The sensible heat flux during spring and summer was significantly better reproduced by the new surface scheme in comparison with the previous scheme. This was mainly because the predicted latent heat flux had been improved and compensating errors in sensible heat flux were thus eliminated. In contrast, simulated and measured sensible heat flux showed some discrepancies during autumn and winter (Fig. 5), especially in September–December 1995. During this period the sensible heat flux from the atmosphere to the surface was significantly underestimated by both model schemes. This was most likely related to an underestimation of fluxes during stable conditions—especially during nighttime (Fig. 9), which was compensated for by an overestimated upward ground heat flux. The large difference between simulated and observed ground heat flux is related to the fact that the observations represent the heat flux at the soil surface whereas the simulations represent the heat flux at the top of the canopy. In fact, the diurnal amplitude of the simulated ground heat flux agreed well with the residual of observed energy balance components (Fig. 9d) and the systematic discrepancy corresponds to the underestimation of sensible heat flux. Too much heat was taken from the soil instead of from the air to balance the negative radiation budget during cold winter nights. This suggests that the aerodynamic coupling between the surface and the atmosphere was too weak and/or the thermal skin layer conductivity was too high. A sensitivity test in which the values for skin layer conductivity and roughness length for heat were varied showed that simulation of both ground heat flux and soil temperatures could be significantly improved. The best result was obtained by increasing the roughness length for heat by a factor of 10 and reducing the skin layer conductivity to 10% of its original value, in the same run (Table 5). The slope of the linear regression between simulated and observed sensible heat flux then improved from 0.73 to 0.88, while for ground heat flux the corresponding value changed from 2.4 to 1.4. The larger value of roughness length for heat is supported by results from Mölder and Lindroth (1999), which show that for the NOPEX area the roughness length for heat is in the same range as that for momentum. The lack of closure in the observed energy balance (Fig. 9b) may be explained by heat storage within the canopy, which is not accounted for in the measurements.

### *e. Soil temperatures*

The prediction of soil temperatures during winter was slightly improved with the new scheme (TESSEL), most

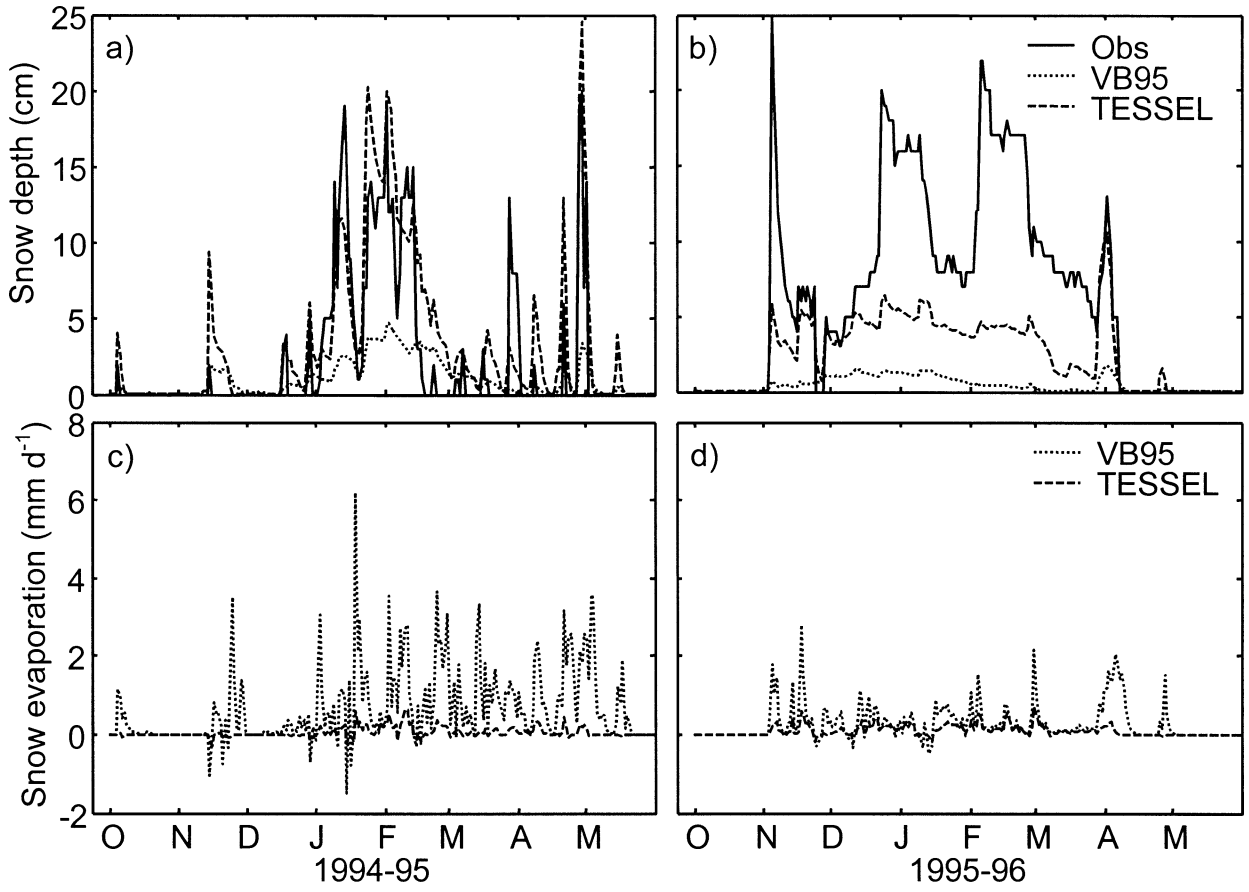


FIG. 8. (a),(b) Simulated and measured (Uppsala Airport) snow depth, and (c),(d) simulated snow evaporation for (left) winter 1994–95 and (right) winter 1995–96.

likely because of changed routines for heat flux between snow and soil. Simulated soil temperatures were generally overestimated during the vegetation period and underestimated during winter by both models (Fig. 10). This could have been caused by too-large values for the soil thermal conductivity and/or the skin layer conductivity. Sensitivity tests showed substantially improved prediction of soil temperature when the skin layer conductivity was decreased (Table 5). The slope of the linear regression between simulated and observed soil temperatures in the uppermost soil layer (0–7 cm) changed from 1.43 to 1.03 when the skin layer conductivity was decreased to 10% of its original value. However, this test also showed that the parameter should be kept at its original value for the snow tiles (high vegetation with snow beneath and snow on low vegetation) in order to accurately simulate snowmelt. Another source of error could be that the assumption of zero heat flux at the lower boundary of the soil profile (2.89 m) was not appropriate for the seasonal timescale. A test simulation was run in which the lower boundary zero heat flux was replaced by an annual heat flux sine wave, estimated from the measured ground heat flux. However, this did not significantly improve the simulated soil temperatures.

### *f. Latent heat flux—The role of transpiration*

The TESSEL scheme improved simulated latent heat flux just after snowmelt, because 1) the reduction of transpiration in the presence of frozen soils was now taken into account and 2) the predicted duration of snow cover had improved (Figs. 8a,b). However, in spring 1996, the soil temperature and moisture measurements indicate that the TESSEL scheme overestimated the duration of soil frost by some weeks, at 28–100-cm depth (Figs. 10 and 11). Grelle et al. (1999) suggested that transpiration in spring and summer 1996 was reduced because of frost-damage of roots and tissues in the foliage. The new scheme indeed correctly reduced the transpiration, but possibly partly for the wrong reason.

The VB95 scheme overestimated latent heat flux as well as transpiration in early summer (Figs. 4 and 12). Results from the TESSEL scheme agreed well with observed values during the same period, most likely as a

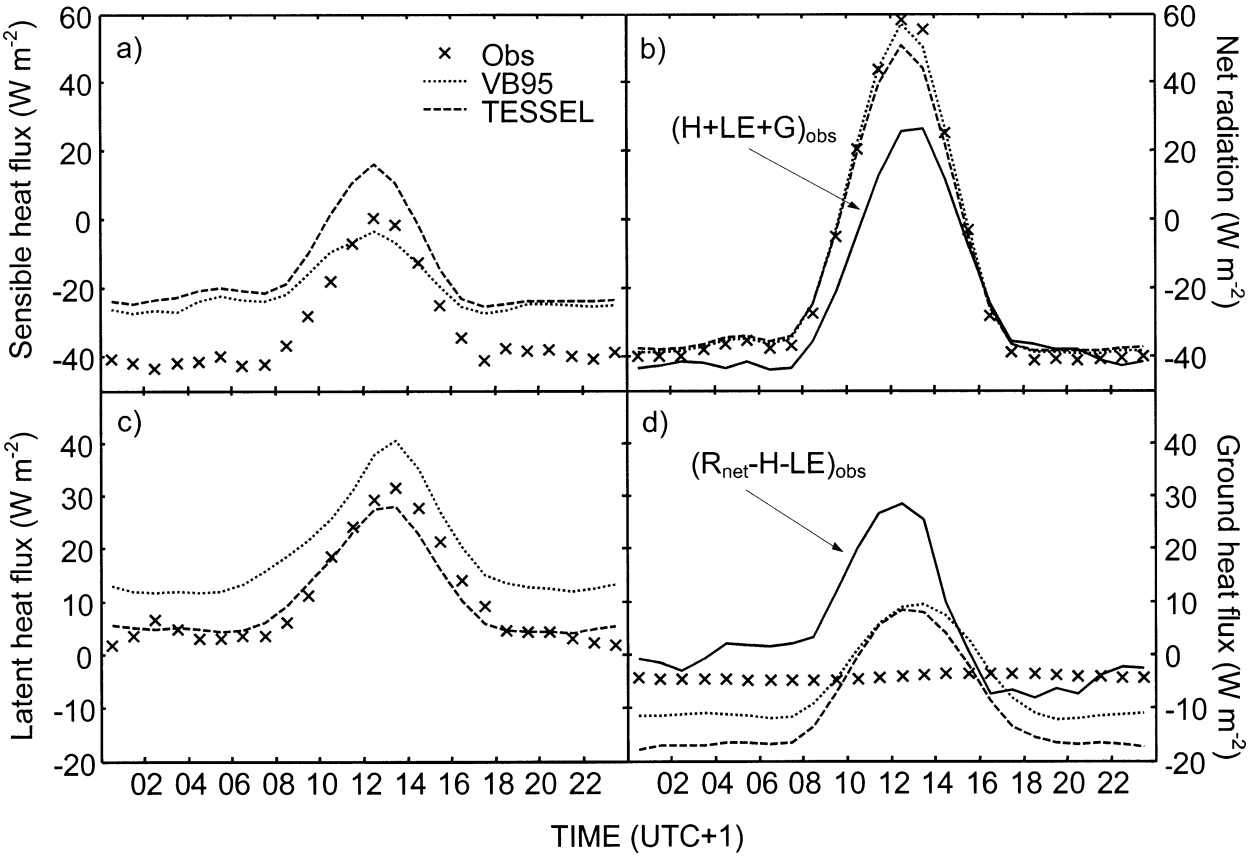


FIG. 9. Surface heat fluxes (turbulent fluxes of sensible and latent heat are positive upward, net radiation and ground heat flux are positive downward), average diurnal course Oct–Dec 1995.

TABLE 5. Linear regression for TESSEL simulations vs NOPEX observations—intercept ($a_0$), slope ($a_1$), coefficient of determination ($r^2$)—and root-mean-square error (rmse), based on daily average values.

| | Net radiation (W m$^{-2}$) | | | | Sensible heat flux (W m$^{-2}$) | | | | Latent heat flux (W m$^{-2}$) | | | | Ground heat flux (W m$^{-2}$) | | | |
|---|---|---|---|---|---|---|---|---|---|---|---|---|---|---|---|---|
| ID* | $r^2$ | $a_0$ | $a_1$ | Rmse | $r^2$ | $a_0$ | $a_1$ | Rmse | $r^2$ | $a_0$ | $a_1$ | Rmse | $r^2$ | $a_0$ | $a_1$ | Rmse |
| (a) | 0.911 | 5.001 | 0.904 | 22.7 | 0.803 | 11.46 | 0.727 | 24.6 | 0.804 | 4.668 | 0.801 | 13.3 | 0.372 | 1.691 | 2.392 | 15.2 |
| (b) | 0.907 | 8.452 | 0.921 | 23.6 | 0.838 | 14.21 | 0.818 | 23.8 | 0.807 | 4.772 | 0.798 | 13.3 | 0.479 | 1.962 | 1.393 | 7.0 |
| (c) | 0.907 | 8.529 | 0.935 | 23.8 | 0.834 | 14.4 | 0.877 | 24.7 | 0.773 | 6.085 | 0.749 | 14.4 | 0.476 | 1.968 | 1.396 | 7.0 |
| (d) | 0.911 | 5.103 | 0.906 | 22.7 | 0.796 | 9.44 | 0.687 | 24.7 | 0.807 | 4.628 | 0.892 | 13.5 | 0.373 | 1.693 | 2.391 | 15.2 |
| (e) | 0.911 | 5.139 | 0.908 | 22.7 | 0.798 | 8.61 | 0.669 | 24.7 | 0.811 | 4.131 | 0.945 | 13.9 | 0.371 | 1.683 | 2.380 | 15.1 |
| (f) | 0.907 | 8.585 | 0.925 | 23.7 | 0.839 | 11.30 | 0.760 | 22.6 | 0.812 | 4.247 | 0.944 | 13.9 | 0.479 | 1.958 | 1.389 | 6.9 |
| | Transpiration (mm day$^{-1}$) | | | | Temperature 0–7 cm (°C) | | | | Temperature 7–28 cm (°C) | | | | Temperature 28–100 cm (°C) | | | |
| | $r^2$ | $a_0$ | $a_1$ | Rmse | $r^2$ | $a_0$ | $a_1$ | Rmse | $r^2$ | $a_0$ | $a_1$ | Rmse | $r^2$ | $a_0$ | $a_1$ | Rmse |
| (a) | 0.857 | 0.215 | 0.712 | 0.39 | 0.958 | −2.27 | 1.423 | 2.81 | 0.967 | −2.41 | 1.433 | 2.52 | 0.983 | −2.23 | 1.439 | 1.99 |
| (b) | 0.850 | 0.223 | 0.719 | 0.39 | 0.971 | 0.086 | 1.038 | 1.04 | 0.971 | −0.16 | 1.062 | 0.99 | 0.930 | −0.29 | 1.087 | 1.28 |
| (c) | 0.851 | 0.219 | 0.657 | 0.43 | 0.971 | 0.027 | 1.031 | 1.00 | 0.970 | −0.21 | 1.055 | 0.97 | 0.927 | −0.33 | 1.077 | 1.27 |
| (d) | 0.845 | 0.261 | 0.832 | 0.38 | 0.958 | −2.28 | 1.420 | 2.78 | 0.967 | −2.42 | 1.429 | 2.50 | 0.982 | −2.23 | 1.433 | 1.96 |
| (e) | 0.860 | 0.260 | 0.900 | 0.39 | 0.958 | −2.28 | 1.417 | 2.77 | 0.967 | −2.42 | 1.426 | 2.49 | 0.983 | −2.22 | 1.430 | 1.94 |
| (f) | 0.852 | 0.270 | 0.906 | 0.40 | 0.971 | 0.068 | 1.034 | 1.02 | 0.971 | −0.18 | 1.058 | 0.97 | 0.929 | −0.30 | 1.080 | 1.27 |

* Simulation identification: (a) default simulation, (b) the skin layer conductivity set to 10% of the original value for all tiles except the snow tiles, (c) as (a) but with the roughness length for heat set equal to the roughness length for momentum, (d) the minimum canopy resistances set to 75% of the original values, (e) as (d) but with a seasonal variation of leaf area index (20% around the original value), and (f) a combination of (b) and (e).

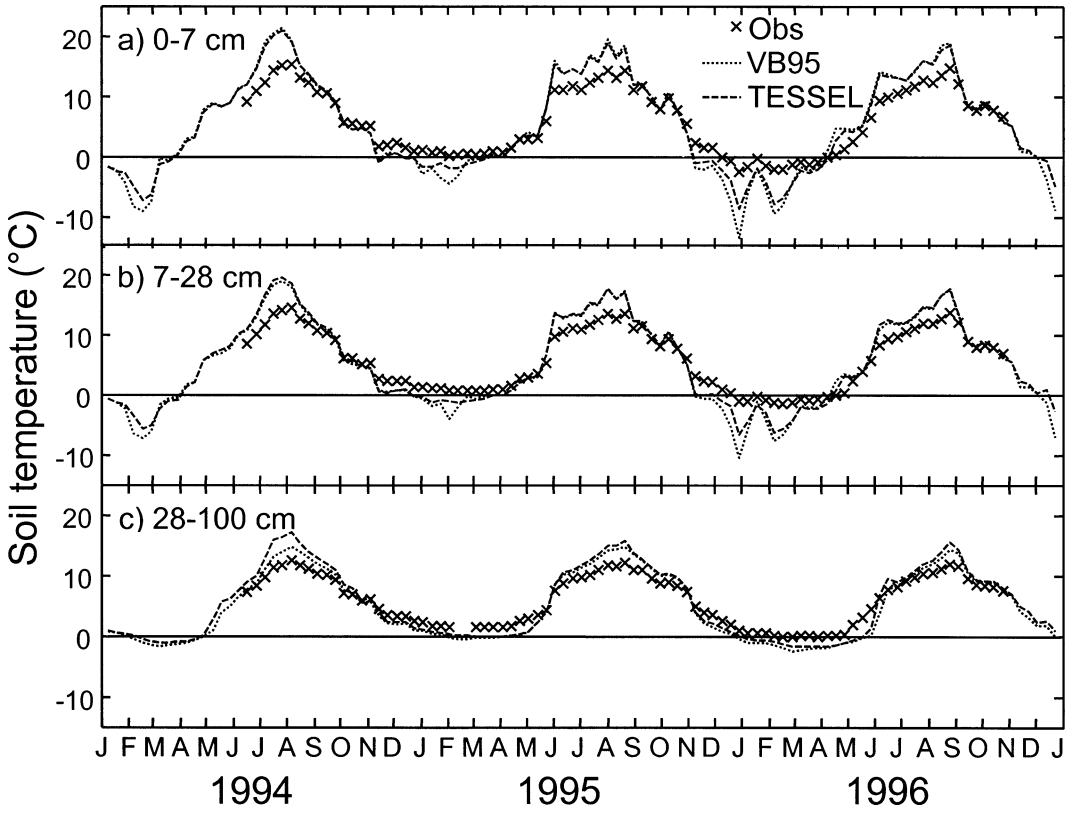


FIG. 10. Simulated and measured soil temperature in model layers at (a) 0–7, (b) 7–28, and (c) 28–100 cm (10-day averages). Measurements from 15 soil profiles were averaged and integrated over the model layer depths to match the simulations.

consequence of the increased value for minimum canopy resistance (Table 3).

The VB95 and TESSEL models reproduced observations well in June–August 1994, when the P–M equation failed (Fig. 4). On the other hand, both land surface schemes, especially TESSEL, underestimated the latent heat flux during the same period in 1995. The results suggest that the control of transpiration by soil moisture on the canopy resistance was efficient in 1994 whereas it was overestimated in 1995. Simulations as well as observations indicated a significant soil water deficit in both 1994 and 1995. The simulated degree of stress related to soil moisture was of similar size in both years. The difference in performance between years may have several explanations:

1) In the ECMWF surface scheme, the water uptake is distributed in the profile according to a fixed root distribution, which will strongly affect the degree of stress. However, the stand average root distribution may deviate from the one assumed and may also vary between years.
2) Some soil–vegetation–atmosphere transfer schemes account for ''compensatory uptake of water,'' which means that root water demand in stressed parts of a soil profile may be compensated for by higher uptake from unstressed parts of the root zone. Jansson et al. (1999) showed that a certain degree of reallocation of the water uptake from stressed parts of the root zone to nonstressed parts was needed to explain observed evaporation, transpiration, and soil water content at the NOPEX Central Tower site in 1994.

Compensatory uptake of water and/or a different root distribution may thus have limited the degree of stress in 1995, which was not accounted for in either of the ECMWF models. The lack of seasonal development of LAI in the model schemes may also contribute to the general pattern of closer agreement between simulated and observed values in spring and early summer followed by underestimation later in the season (Fig. 12). For a forest of mixed pine and spruce, seasonal LAI may vary by 10%–20% (E. Cienciala 2000, personal communication), which would correspond to about 10 W $m^{-2}$ in summertime latent heat flux for the range of the data presented in Fig. 4.

In contrast to VB95, TESSEL accounts for the impact of diurnal variation in vapor pressure deficit on transpiration and thus on latent heat flux. The results indicate that the average diurnal course of latent heat flux simulated by TESSEL was slightly better during the summer period than that simulated with the VB95 scheme (Fig. 13). The new scheme reproduced better the rate of change of latent heat flux in morning and evening.

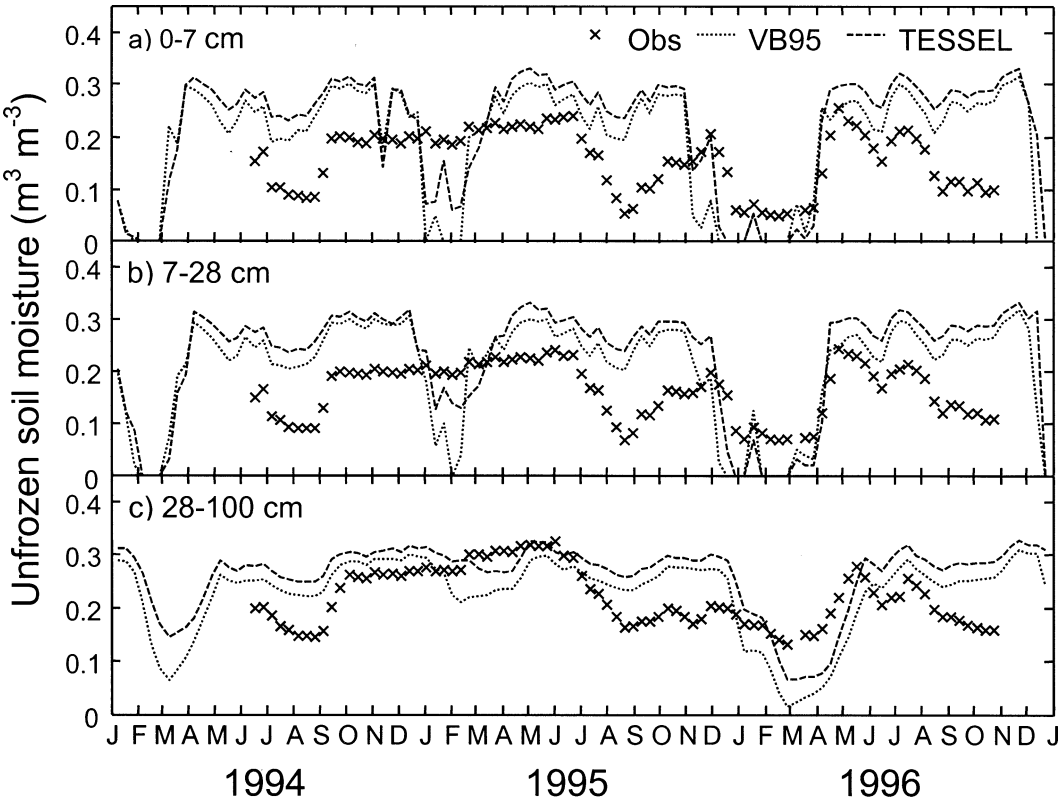


FIG. 11. Simulated and measured unfrozen soil moisture in model layers at (a) 0–7, (b) 7–28, and (c) 28–100 cm (10-day averages). Measurements from 15 soil profiles were averaged and integrated over the model layer depths to match the simulations.

During the period of concern, the relative increase of canopy resistance due to soil moisture stress in the VB95 model was about twice as high as in the TESSEL model (see $f_2$, Fig. 14). The stress with respect to radiation ($f_1$) during midday was similar in both models, although the response function had been modified. The stress function due to vapor pressure deficit ($f_3$) increased the canopy resistance by about 50% in the TESSEL scheme.

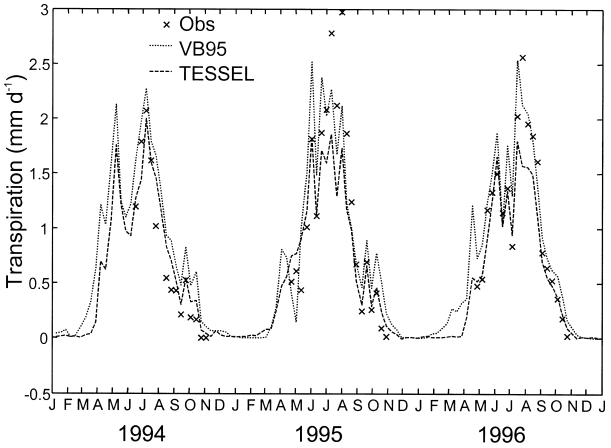


FIG. 12. Simulated transpiration and measured sap flow (10-day averages).

Soil moisture stress had thus partly been replaced by stress related to vapor pressure deficit, which has a different temporal pattern. The total stress in the VB95 model exceeded that in the TESSEL model (Fig. 14). However, the net uptake of water was still higher in the VB95 model, because the ''unstressed transpiration'' governed by the minimum canopy resistance value was higher than in the TESSEL model.

A sensitivity test with the TESSEL scheme showed that a reduction of the minimum canopy resistance by 25% reduced the discrepancies between simulated and observed fluxes, especially in summer 1995 and summer 1996. The slope of the linear regression between simulated and observed values increased from 0.80 to 0.89 and from 0.71 to 0.83 for latent heat flux and transpiration, respectively (Table 5). Further improvements were obtained when, in addition, a seasonal variation in LAI (20% around the mean, with a minimum in February and a maximum in August) was introduced. The regression slopes then improved to 0.945 and 0.9 for latent heat flux and transpiration, respectively (Table 5).

### *g. Evaporation components*

Total evaporation over the period of concern decreased from 1429 mm in VB95 to 1057 mm in the TESSEL simulations (1056 days). This could mainly be

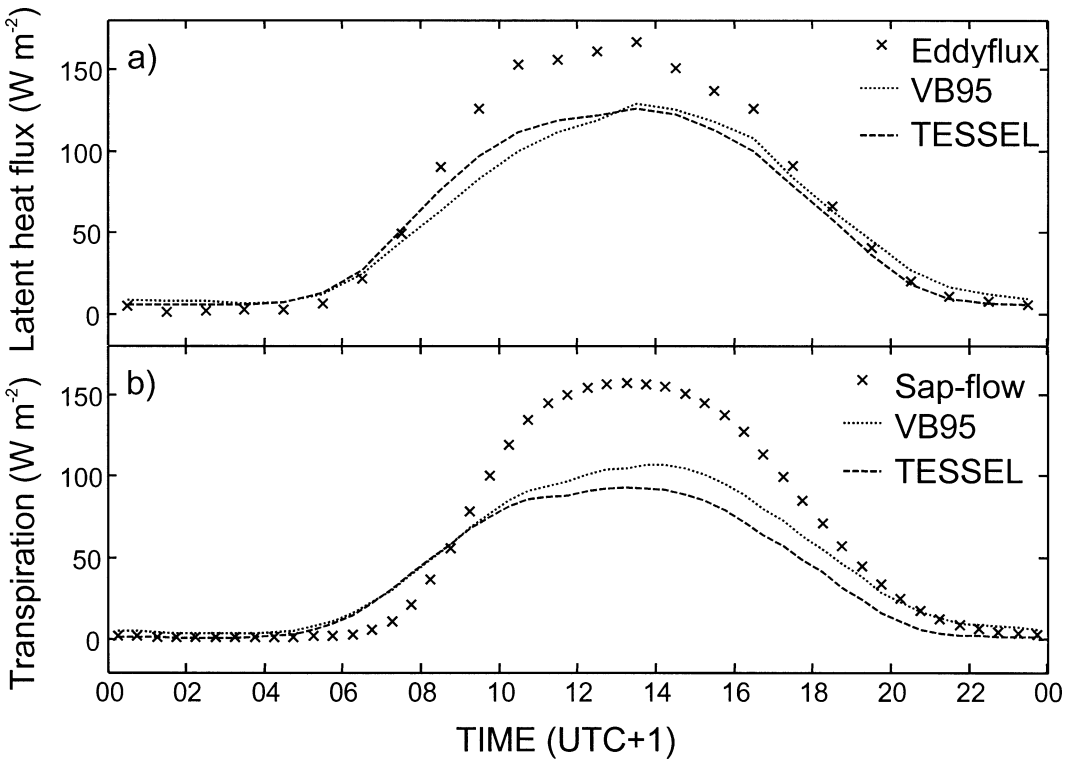


FIG. 13. (a) Simulated and measured latent heat flux and (b) simulated transpiration and observed sap flow, average diurnal course 4 Jul–31 Aug 1995.

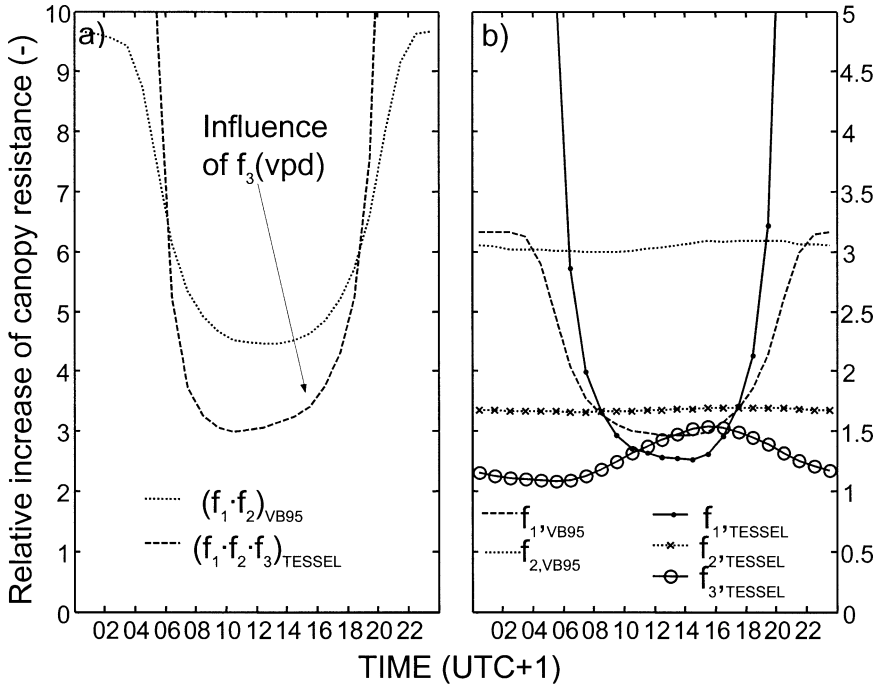


FIG. 14. (a) Relative increase of canopy resistance in the VB95 and TESSEL simulations, and (b) their components representing stress due to solar radiation ($f_1$), soil moisture stress ($f_2$), and vapor pressure deficit ($f_3$), average diurnal course 4 Jul–31 Aug 1995.

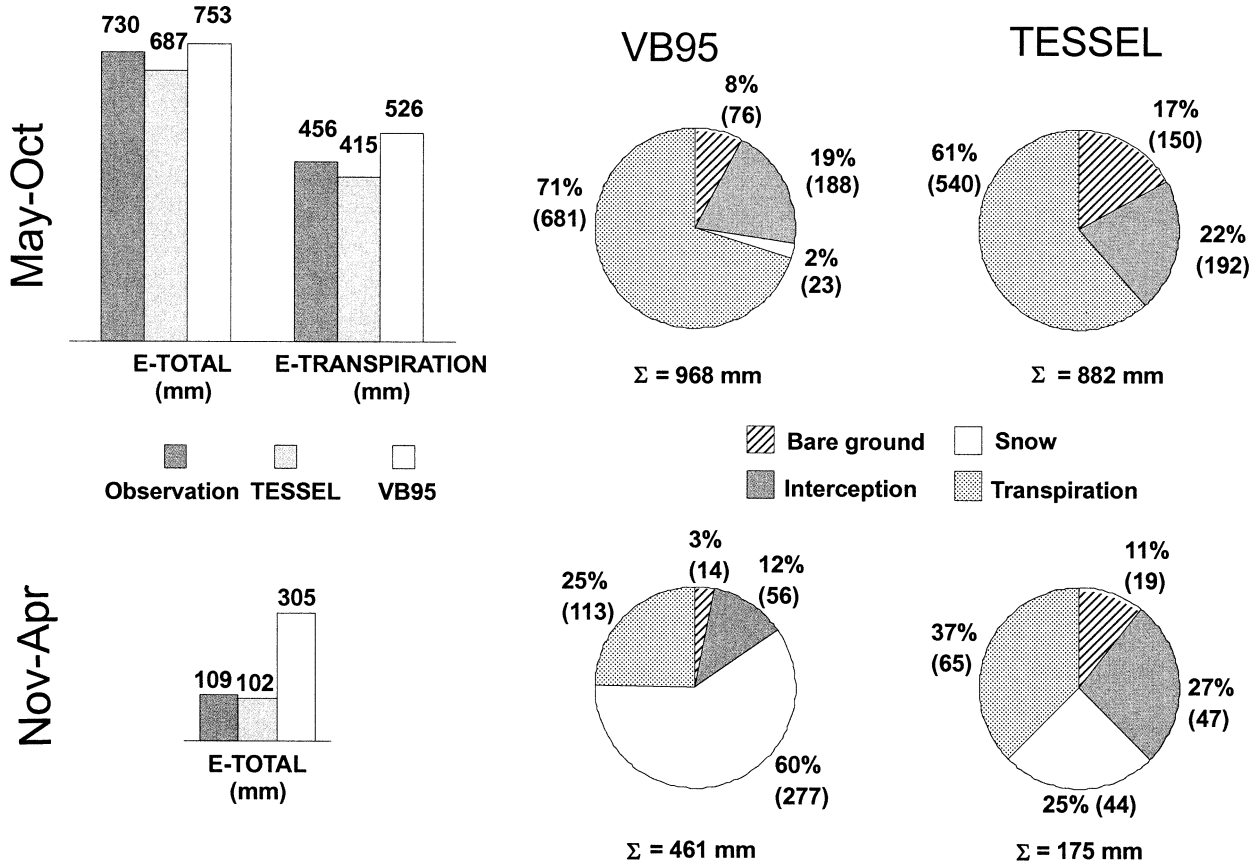


FIG. 15. (left) Total evaporation ($E$) and transpiration simulated by the VB95 and TESSEL models and observed with eddy-correlation ($E$-total) and sap flow ($E$-transpiration), based on 435 days May–Oct and 358 days Nov–Apr 1994, 1995, and 1996. (right) Evaporation from different components simulated by the VB95 and TESSEL models, based on 552 days May–Oct and 543 days Nov–Apr 1994, 1995, and 1996.

attributed to decreased evaporation from snow (−233 mm) and transpiration (−179 mm) and thus to the changed routines governing these components (Fig. 15). In contrast, evaporation from bare soil increased significantly (+79 mm), as a result of the changed formulation for bare soil evaporation. Comparison with available observations indicates that the TESSEL simulation reduced evaporation and especially transpiration too much in May–October (Fig. 15). However, because of the increased bare soil evaporation the proportion of transpiration decreased from 71% (VB95) to 61% (TESSEL), which compared better to the relation between observed transpiration (sap flow) and total evaporation (eddy-correlation) during this period (62%). Total evaporation simulated by the TESSEL model agreed well with observations in November–April. Evaporation from intercepted water did not change much, but increased when expressed as a proportion of total evaporation because of the general reduction of evaporation, especially in winter.

## 4. Conclusions

Single-column runs showed that measured seasonal variations in surface energy fluxes for a Scandinavian boreal forest were significantly better reproduced by the new ECMWF surface scheme (TESSEL) in comparison with the old version. The major reasons for this are the new parameterizations of winter processes and transpiration control, which improved the simulated partitioning of net radiation into sensible and latent heat flux.

Evaporation during winter was greatly overestimated by the old scheme because of an overestimated evaporation from snow. The significant improvement in the simulated winter evaporation in the TESSEL model confirms the results obtained by van den Hurk et al. (2000) that a more realistic representation of evaporation from snow lying under vegetation was achieved when the extinction of turbulent exchange under the canopy was taken into account. The introduction of a function that limits transpiration in frozen soils also improved the simulated evaporation in spring. However, on some occasions an overestimation of the duration of soil frost might have compensated for other soil frost–induced processes affecting water uptake by roots.

Despite the improved simulation of evaporation in winter, downward sensible heat flux was still somewhat underestimated during winter, especially at night. This

was compensated for by an overestimated upward ground heat flux. The results indicate that the aerodynamic coupling between the surface and the atmosphere was too weak and/or the skin layer conductivity was too high to represent the NOPEX site. This was also confirmed by sensitivity tests.

The introduction of a higher canopy resistance representing typical boreal forest reduced the total simulated evaporation during summer to more realistic values. The TESSEL scheme also simulated diurnal variation in evapotranspiration with better accuracy, because of the inclusion of a canopy resistance response to vapor pressure deficit. The proportion of transpiration to total evaporation during summer was in much better agreement with the observations, even though the total amount of evaporation was somewhat underestimated. Transpiration was underestimated in late summer, probably because seasonal development of LAI and compensatory uptake of water were not accounted for in the model scheme. Even though total evaporation was reduced, the change from a relative humidity approach to a surface resistance approach in TESSEL considerably increased evaporation from bare soil.

Sensitivity tests showed that the ECMWF surface scheme could be further improved with respect to boreal forest areas by introducing seasonal variations in vegetation properties (Betts et al. 1998b) and by changing the minimum canopy resistance. Model performance would also be improved by modification of the stability correction for stable conditions and by calibration of the parameter for skin layer conductivity.

*Acknowledgments.* Thanks are due to Dr. J. Seibert and Dr. E. Kellner (Uppsala University) for making data available on precipitation and soil moisture/temperature. Meteorological data from Uppsala Airport were obtained from the Swedish Meteorological and Hydrological Institute (SMHI). We also kindly thank Prof. P-E. Jansson (KTH, Stockholm), Prof. N. Jarvis (SLU, Uppsala), and Prof. A. Beljaars (ECMWF, Reading) for valuable discussions and comments. This project was funded by the Swedish Natural Science Research Council.

## APPENDIX

### Instruments and Data-Processing Functions

All variables and data-processing functions used for the preparation of the meteorological forcing are summarized in Table A1. Linear regression functions used for the transformation of climatic variables at Uppsala airport to the Norunda site are listed in Table A2. Additional functions used are listed in Table A3, and the instruments are listed in Table A4. Instruments used for the validation data are summarized in Table A5.

TABLE A1. Variables used for the meteorological forcing.

| Forcing variables | Source variables | | Capture fraction[d] | |
|---|---|---|---|---|
| Variable | Name | Location | | Data processing |
| Air temperature (K) | $T_{CTS}$ (°C) | CTS[a] 35 m | 83 (97)% | 1) Weighted average of two sensors at 31.7 and 36.9 m, 2) $T'_{CTS} = T_{CTS} + 273.15$ |
| | $T_{UA}$ (°C) | UA[b] 1.5 m | 17 (3)% | 1) Scaled by linear regression between $T_{CTS}$ and $T_{UA}$ (cf. Table A2), 2) $T'_{UA} = T_{UA} + 273.15$ |
| Wind speed (m s$^{-1}$) | $U_{CTS}$ (m s$^{-1}$) | CTS 35 m | 76 (88)% | |
| | $U_{UA}$ (m s$^{-1}$) | UA 10 m | 24 (12)% | Scaled by linear regression between $U_{CTS}$ and $U_{UA}$ (cf. Table A2) |
| Specific air humidity (kg kg$^{-1}$) | $q_{CTS,1}$ (g kg$^{-1}$) | CTS 35 m | 28 (32)% | 1) $q'_{CTS,1} = q_{CTS,1} \times 10^{-3}$, 2) larger drifts in the calibration were scaled by comparison of moving averages (96 h) between $q'_{CTS,1}$ *and* $q_{UA}$ (cf. Table A2) |
| | $mr_{CTS}$ (g kg$^{-1}$) | CTS 35 m | 53 (61)% | 1) $q_{CTS,2} = (mr_{CTS} \times 10^{-3})/(1 + mr_{CTS} \times 10^{-3})$ 2) average of two sensors at 31.7 and 36.9 m |
| | $e_{UA}$ (Pa) | UA 1.5 m | 17 (6)% | 1) $q_{UA} = (0.622e_{UA})/[(P_{UA} - e_{UA}) + 0.622e_{UA}]$ 2) scaled by linear regression between $q_{CTS,2}$ and $q_{UA}$ (cf. Table A2) |
| | $q_{sat}$ (kg kg$^{-1}$) | Estimated | 2 (1)% | Monteith and Unsworth (1990), cf. Table A3 |
| Atmospheric pressure (Pa) | $Pa_{CTS}$ (Pa) | CTS 2 m | 83 (97)% | $Pa'_{CTS} = Pa_{CTS} - (33 \text{ m} \times 8 \text{ Pa m}^{-1})$ |
| | $Pa_{UA}$ (Pa) | UA 1.5 m | 17 (3)% | Scaled by linear regression between $Pa'_{CTS}$ and $Pa_{UA}$ (cf. Table A2) |
| Downward shortwave radiation (W m$^{-2}$) | $R_{IS,\,CTS}$ (W m$^{-2}$) | CTS 102 m | 83 (97)% | |
| | $R_{IS,\,EST}$ (W m$^{-2}$) | Estimate | 17 (3)% | Ångström (1924), cf. Table A3 |
| Downward longwave radiation (W m$^{-2}$) | $R_{IL,\,CTS\,68}$ (W m$^{-2}$) | CTS 68 m | 79 (94)% | |
| | $R_{IL,\,EST}$ (W m$^{-2}$) | Estimate | 21 (6)% | Konzelmann et al. (1994), cf. Table A3 |
| Precipitation (mm h$^{-1}$) | $P_{CTS}$ [mm (10 min)$^{-1}$] | CTS 1.5 m | 37 (42)% | Accumulation within hours |
| | $P_{MMO}$ [mm (10 min)$^{-1}$] | MMO[c] 1.5 m | 6 (7)% | 1) Accumulation within hours, 2) multiplied by a factor of 1.1 based on comparison of accumulated values of $P_{CTS}$ and $P_{MMO}$ from common time periods |
| | $P_{UA}$ [mm (12 h)$^{-1}$] | UA 1.5 m | 57 (51)% | 1) Equally divided between hours with observed precipitation events, 2) correction of systematic errors following Eriksson (1983), cf. Table A3 |

[a] CTS = NOPEX Central Tower Station.
[b] UA = Uppsala Airport.
[c] MMO = Marsta Meteorological Observatory.
[d] Percentage of time in the final dataset during Jan 1994–Dec 1996 (validation period, Jun 1994–Dec 1996).

TABLE A2. Transformations of climatic variables from Uppsala Airport to Norunda.

| Variable (unit) | Function | $r^2$ | $N$ |
|---|---|---|---|
| Air temperature (°C) | $T_{CTS} = 0.0317 + 0.947T_{UA}$ | 0.961 | 21 886 |
| Wind speed (m s$^{-1}$) | $U_{CTS} = 1.356 + 0.290U_{UA}$ | 0.433 | 19 956 |
| Atmospheric pressure (Pa) | $Pa'_{CTS} = 257.5 + 0.991Pa_{UA}$ | 0.992 | 21 887 |
| Air humidity (kg kg$^{-1}$) | $q'_{CTS,2} = 1.96 \times 10^{-4} + 0.900q_{UA}$ | 0.951 | 13 964 |

TABLE A3. Functions used in the preparation of the meteorological forcing data.

| Variable | Function |
|---|---|
| Saturated vapor pressure (Pa) | $e_s = \begin{cases} 10^{(12.5553-2667)/T_{CTS}} & T_{CTS} \le 273.15\ \text{K} \\ 10^{(11.4051-2353)/T_{CTS}} & T_{CTS} > 273.15\ \text{K} \end{cases}$ (Monteith and Unsworth 1990) |
| Downward longwave radiation (W m$^{-2}$) | $R_{IL,EST} = \left\{\left[0.23 + 0.484\left(\frac{e_{CTS}}{T_{CTS}}\right)^{1/8}\right](1 - N_{UA}^4) + 0.952N_{UA}^4\right\}\sigma T_{CTS}^4$ (Konzelmann et al. 1994)* |
| Downward shortwave radiation (W m$^{-2}$) | 1) $R_{IS,POT} = 1360\left(\frac{S_z}{S_x^2 + S_y^2 + S_z^2}\right)$, $S_x = \sin\Phi\cos\Lambda$, $S_y = \cos\Phi\cos\Lambda$, $S_z = \sin\Lambda$ where the azimuth angle $\Phi$ and the elevation angle $\Lambda$ of the sun are given by the latitude, the longitude, and the time and day of year (Monteith and Unsworth 1990) |
| | 2) $R_{IS,EST} = R_{IS,POT}(0.72 - 0.5N_{UA})$ (Ångström 1924)* |
| Precipitation correction for systematic errors | $P'_{UA} = P_{UA} \times \begin{cases} 1.15 & T_{UA} \le -2°\text{C} \\ 1.11 - 0.02T_{UA} & -2°\text{C} < T_{UA} < 2°\text{C} \\ 1.07 & T_{UA} \ge 2°\text{C} \end{cases}$ (Eriksson 1983) |

* $N_{UA}$ = Cloud cover observed at UA.

TABLE A4. Instruments used for the meteorological forcing data.

| Variable | Name | Instrument |
|---|---|---|
| Air temperature | $T_{CTS}$ | Copper–constantan thermocouple (radiation-shielded and ventilated; In Situ, Ockelbo, Sweden) |
| | $T_{UA}$ | SMHI* |
| Wind speed | $U_{CTS}$ | Sonic anemometer (Gill Instruments Solent Basic, Lymington, United Kingdom) |
| | $U_{UA}$ | SMHI* |
| Specific air humidity | $q_{CTS,1}$ | Gas analyzer (LI-COR 6262, Lincoln, NE) |
| | $mr_{CTS}$ | Gas analyzer (LI-COR 6262, Lincoln, NE) |
| | $e_{UA}$ | SMHI* |
| Atmospheric pressure | $Pa_{CTS}$ | Indoors pressure sensor (Vaisala PTA 427, Helsinki, Finland) |
| | $Pa_{UA}$ | SMHI* |
| Downward shortwave radiation | $R_{IS,\ CTS}$ | Pyranometer (Kipp and Zonen CM21, Delft, Netherlands) |
| Downward longwave radiation | $R_{IL,\ CTS\ 68}$ | Net radiometer (Dr. Bruno Lange LXV055, Berlin, Germany) |
| Precipitation | $P_{CTS}$ | Rain gauge (In Situ IS200 W, Ockelbo, Sweden) |
| | $P_{MMO}$ | Rain gauge (In Situ IS200 W, Ockelbo, Sweden) |
| | $P_{UA}$ | Rain gauge, SMHI* |

* Weather observations maintained by the Swedish Meteorological and Hydrological Institute (SMHI), Norrköping, Sweden.

TABLE A5. Instruments used for the validation data.

| Variable | Instrument |
|---|---|
| Latent heat flux (W m$^{-2}$) | Sonic anemometer (Gill Instruments Solent Basic, Lymington, United Kingdom), and gas analyzer (LI-COR 6262, Lincoln, NE) |
| Sensible heat flux (W m$^{-2}$) | Sonic anemometer (as above) |
| Net radiation (W m$^{-2}$) | Net radiometer (Dr. Bruno Lange LXV055, Berlin, Germany) |
| Soil heat flux (W m$^{-2}$) | Heat-flux plates (REBS HFT-1, Seattle, WA) |
| Tree sap flow (mm day$^{-1}$) | Tissue-heat-balance sap-flow meter (Environmental Measuring Systems P609.2, Brno, Czech Republic) |
| Soil temperature (°) | Thermocouple (In Situ, Ockelbo, Sweden) |
| Soil moisture (m$^3$ m$^{-3}$) | TDR (Tektronix 1502B, Pittsfield, MA) |

## REFERENCES


Ångström, A., 1924: Solar and terrestrial radiation. *Quart. J. Roy. Meteor. Soc.,* **50,** 121–125.

Beljaars, A. C. M., and A. A. M. Holtslag, 1991: Flux parameterization over land surfaces for atmospheric models. *J. Appl. Meteor.,* **30,** 327–341.

Betts, A. K., P. Viterbo, and A. C. M. Beljaars, 1998a: Comparison of the land-surface interaction in the EMCWF reanalysis model with the 1987 FIFE data. *Mon. Wea. Rev.,* **126,** 186–198.

——, ——, ——, H.-L. Pan, S.-Y. Hong, M. Goulden, and S. Wofsy, 1998b: Evaluation of land surface interaction in ECMWF and NCEP/NCAR reanalysis models over grassland (FIFE) and boreal forest (BOREAS). *J. Geophys. Res.,* **103D,** 23 079–23 085.

——, M. Goulden, and S. Wofsy, 1999: Controls on evaporation in a boreal spruce forest. *J. Climate,* **12,** 1601–1618.

Bonan, G. B., D. Pollard, and S. L. Thompson, 1992: Effects of boreal forest vegetation on global climate. *Nature,* **359,** 716–718.

——, F. S. Chapin, and S. L. Thomson, 1995: Boreal forest and tundra ecosystems as components of the climate system. *Climatic Change,* **29,** 145–167.

Bosveld, F., A. van Ulden, and A. C. M. Beljaars, 1999: A comparison of ECMWF re-analysis data with fluxes and profiles observed in Cabauw. ECMWF ERA-projects Series, No. 8, 50 pp. [Available from European Centre for Medium-Range Weather Forecasts, Shinfield Park, Reading, Berkshire RG2 9AX, United Kingdom.]

Chen, T., and Coauthors, 1997: Cabauw experimental results from the Project for Intercomparison of Land-surface Parameterization Schemes (PILPS). *J. Climate,* **10,** 1194–1215.

Cienciala, E., J. Kucera, and A. Lindroth, 1999: Long-term measurements of stand water uptake in Swedish boreal forest. *Agric. For. Meteor.,* **98–99,** 547–554.

Douville, H., and J.-F. Royer, 1997: Influence of the temperate and boreal forests on the Northern Hemisphere climate in the Météo-France climate model. *Climate Dyn.,* **13,** 57–74.

——, J.-F. Mahfouf, S. Saarinen, and P. Viterbo, 1998: The ECMWF surface analysis: Diagnostics and prospects. ECMWF Tech. Memo. 258, 51 pp. [Available from European Centre for Medium-Range Weather Forecasts, Shinfield Park, Reading, Berkshire RG2 9AX, United Kingdom.]

Eriksson, B., 1983: Data concerning the precipitation climate of Sweden: Normal values for the period 1951–80. Rep. 1983: 28, SMHI, Norrköping, Sweden, 92 pp.

Grelle, A., 1997: Long-term water and carbon dioxide fluxes from a boreal forest: Methods and applications. Ph.D. thesis, Silvestria 28, Acta Universitaris Agriculturae Sueciae, 80 pp. [Available from Department for Production Ecology, Box 7042, S-750 07 Uppsala, Sweden.]

——, and A. Lindroth, 1996: Eddy-correlation system for long-term monitoring of fluxes of heat, water vapour and $CO_2$. *Global Change Biol.,* **2,** 297–307.

——, ——, and M. Mölder, 1999: Seasonal variation of boreal forest surface conductance and evaporation. *Agric. For. Meteor.,* **98–99,** 563–578.

Halldin, S., L. Gottschalk, A. A. van den Griend, S.-E. Gryning, M. Heikinheimo, U. Högström, A. Jochum, and L.-C. Lundin, 1998: NOPEX—a Northern Hemisphere climate processes land surface experiment. *J. Hydrol.,* **212–213,** 172–187.

——, S. E. Gryning, L. Gottschalk, A. Jochum, L.-C. Lundin, and A. A. van de Griend, 1999: Energy, water and carbon exchange in a boreal forest—NOPEX experiences. *Agric. For. Meteor.,* **98–99,** 5–29.

Henderson-Sellers, A., 1996: Soil moisture simulation: Achievements of the RICE and PILPS intercomparison workshop and future directions. *Global Planet. Change,* **13,** 99–115.

——, Z. L. Yang, and R. E. Dickinson, 1993: The Project for Intercomparison of Land-surface Parameterization Schemes. *Bull. Amer. Meteor. Soc.,* **74,** 1335–1349.

Jansson, P.-E., E. Cienciala, A. Grelle, E. Kellner, A. Lindahl, and M. Lundblad, 1999: Simulated evapotranspiration from the Norunda forest stand during the growing season of a dry year. *Agric. For. Meteor.,* **98–99,** 621–628.

Kellner, E., P.-E. Jansson, A. Lindahl, M. Stähli, K. Hessel, J. Eriksson, and L.-C. Lundin, 1999: The influence of soil moisture dynamics on transpiration at the CTS pine stands. *Agric. For. Meteor.,* **98–99,** Documented dataset on appended CD-ROM.

Konzelmann, T., R. S. W. van de Wal, W. Greuell, R. Bintanja, E. A. C. Henneken, and A. Abe-Ouchi, 1994: Parameterization of global and longwave incoming radiation for the Greenland Ice Sheet. *Global Planet. Change,* **9,** 143–164.

Lafleur, P. M., J. H. McCaughey, D. W. Joiner, P. A. Barlett, and D. E. Jelinski, 1997: Seasonal trends in energy, water, and carbon dioxide fluxes at a northern boreal wetland. *J. Geophys. Res.,* **102D,** 29 009–29 020.

Lundin, L.-C., and Coauthors, 1999: Continuous long-term measurements of soil–plant–atmosphere variables at a forest site. *Agric. For. Meteor.,* **98–99,** 53–73.

Mahfouf, J. F., and J. Noilhan, 1991: Comparative study of various formulations from bare soil using in situ data. *J. Appl. Meteor.,* **30,** 1354–1365.

Monteith, J. L., 1965: Evaporation and the atmosphere. *The State and Movement of Water in Living Organisms: 19th Symposium of the Society for Experimental Biology,* G. E. Fogg, Ed., Company of Biologists, 205–234.

——, and M. Unsworth, 1990: *Principles of Environmental Physics.* 2d ed. Edward Arnold, 291 pp.

Mölder, M., and A. Lindroth, 1999: Thermal roughness length of a boreal forest. *Agric. For. Meteor.,* **98–99,** 659–670.

——, A. Grelle, A. Lindroth, and S. Halldin, 1999a: Flux–profile relationships over a boreal forest—roughness sublayer corrections. *Agric. For. Meteor.,* **98–99,** 645–658.

——, S. Halldin, and A. Lindroth, 1999b: Characterization of the lowest 100 m of the boundary layer and the radiation budget of the surface. *Agric. For. Meteor.,* **98–99,** Documented dataset on appended CD-ROM.

Penman, H. L., 1953: The physical basis of irrigation control. *Report of the 13th International Horticultural Congress 1952,* P. M. Synge, Ed., Vol. II, Royal Horticultural Society London, 913–924.

Schmid, H. P., 1994: Source areas for scalars and scalar fluxes. *Bound.-Layer Meteor.,* **67,** 293–318.

Seibert, J., and A.-S. Morén, 1999: Reducing systematic errors in rainfall measurements using a new type of gauge. *Agric. For. Meteor.,* **98–99,** 341–348.

Thomas, G., and P. R. Rowntree, 1992: The boreal forests and climate. *Quart. J. Roy. Meteor. Soc.,* **118,** 469–497.

van den Hurk, B. J. J. M., P. Viterbo, A. C. M. Beljaars, and A. K. Betts, 2000: Offline validation of the ERA40 surface scheme. ECMWF Tech. Memo. 295, 42 pp. [Available from European Centre for Medium-Range Weather Forecasts, Shinfield Park, Reading, Berkshire RG2 9AX, United Kingdom.]

Verseghy, D. L., 2000: The Canadian Land Surface Scheme (CLASS): Its history and future. *Atmos.–Ocean,* **38,** 1–13.

Viterbo, P., and A. C. M. Beljaars, 1995: An improved land surface parameterization scheme in the ECMWF model and its validation. *J. Climate,* **8,** 2716–2748.

——, and A. K. Betts, 1999: Impact on ECMWF forecasts of changes to the albedo of the boreal forests in the presence of snow. *J. Geophys. Res.,* **104D,** 27 803–27 810.

——, A. C. M. Beljaars, J.-F. Mahfouf, and J. Teixeira, 1999: The representation of soil moisture freezing and its impact on the stable boundary layer. *Quart. J. Roy. Meteor. Soc.,* **125,** 2401–2426.